Research Square

Preprints are preliminary reports that have not undergone peer review.
They should not be considered conclusive, used to inform clinical practice,
or referenced by the media as validated information.

Role of ferroptosis in hippocampal neurons induced by Mex3c gene deletion in the pathogenesis of neurodevelopmental disorders

Hui Cai
Dong Liu
Zhicheng Dai
Zeli Su
lianghong Ma
Yong Du
episkey-ld@nxmu.edu.cn

Research Article

Keywords: Mex3c, Neurodevelopmental disorders, Ferroptosis, GPX4, Hippocampal neurons, Ferrostatin-1

Posted Date: November 3rd, 2026

DOI: https://doi.org/10.21203/rs.3.rs-11300924/v1

License: This work is licensed under a Creative Commons Attribution 4.0 International License.
Read Full License

Additional Declarations: No competing interests reported.

Abstract

Introduction:

Neurodevelopmental disorders (NDDs) are a heterogeneous group of central nervous system disorders that are strongly influenced by genetic alterations. The RNA-binding protein and E3 ubiquitin ligase MEX3C plays an important role in neurodevelopment. However, its precise contribution to NDD pathogenesis and whether it regulates neuronal ferroptosis remain unclear.

Methods

To investigate the role of *Mex3c* in NDDs, we generated *Mex3c* knockout (KO) mice using CRISPR/Cas9 technology and conducted a series of behavioral tests, histological analyses, and molecular assays. Behavioral phenotyping included the open-field test (OFT), light–dark box test (LDB), and novel object recognition test (NOR). Histological assessments included Nissl staining and NeuN immunohistochemistry to evaluate neuronal injury in the CA1, CA3, and dentate gyrus (DG) regions of the hippocampus. Molecular and biochemical evaluations included Western blotting, immunofluorescence staining, and analysis of ferroptosis- and oxidative stress-related markers, including GPX4, FTH1, NCOA4, reactive oxygen species (ROS), malondialdehyde (MDA), and glutathione (GSH). In addition, the ferroptosis-specific inhibitor Ferrostatin-1 (Fer-1) was administered for in vivo rescue experiments.

Results

Mex3c KO mice exhibited pronounced NDD-like phenotypes, including anxiety-like behaviors and impaired recognition memory. These behavioral abnormalities were accompanied by neuronal loss and structural damage across multiple hippocampal subregions. Mechanistic analyses revealed that *Mex3c* deficiency induced ferroptosis in hippocampal neurons, as evidenced by reduced expression of GPX4 and FTH1, increased NCOA4 expression, GSH depletion, and excessive accumulation of ROS and MDA. Pharmacological treatment with Fer-1 markedly suppressed hippocampal ferroptosis and oxidative stress, restored neuronal density, and effectively reversed anxiety-like behaviors and cognitive deficits in *Mex3c* KO mice.

Conclusion

Our findings suggest that *Mex3c* gene deletion disrupts hippocampal antioxidant defense and iron homeostasis through downregulation of GPX4, thereby triggering neuronal ferroptosis and contributing to anxiety-like behavior and recognition memory impairment in mice. These results support *Mex3c* as a potential susceptibility gene for NDDs and highlight the *Mex3c*/GPX4/ferroptosis axis as a potential therapeutic target for neurodevelopmental disorders.

1.Introduction

Neurodevelopmental disorders (NDDs) comprise a heterogeneous group of central nervous system disorders that arise during critical periods of nervous system development and are primarily characterized by abnormalities in cognition, emotion, and adaptive behavior [1]. Clinically, NDDs, represented by autism spectrum disorder (ASD) and intellectual disability, often have an insidious onset and persist throughout life, resulting in irreversible impairments in social functioning in affected children[2, 3]. Although the pathogenesis of NDDs is highly complex, accumulating evidence in recent years has consistently demonstrated that genetic factors, particularly deletions or mutations of specific genes, are major etiological contributors to NDDs[4, 5]. Currently, the clinical diagnosis of NDDs still relies heavily on behavioral scale assessments [6], while specific molecular biomarkers remain lacking. Moreover, existing interventions are largely aimed at alleviating symptoms, and effective etiological or targeted therapies have yet to be established [6]. Therefore, elucidating the key molecular regulatory networks and mechanisms of neuronal injury involved in the onset and progression of NDDs is of considerable scientific and clinical importance for identifying novel diagnostic biomarkers and specific therapeutic targets.

MEX3C (mex-3 RNA binding family member C) is a highly conserved member of the MEX3 family of RNA-binding proteins, which comprises MEX3A, MEX3B, MEX3C, and MEX3D [7]. The MEX3C protein contains two N-terminal K homology (KH) RNA-binding domains and a C-terminal RING domain[8], conferring both RNA-binding activity and E3 ubiquitin ligase-related functions. Through these properties, MEX3C participates in the regulation of target RNA stability, protein expression, and cellular homeostasis[9]. Previous studies have demonstrated that *Mex3c* is closely associated with embryonic development, energy metabolism, and nervous system development[10]. In particular, during embryogenesis, *Mex3c* is highly expressed in the central nervous system and neural tube, and its dysfunction can affect the proliferation and survival of neuroepithelial cells [11]. Our previous study further demonstrated that *Mex3c* deficiency leads to abnormal neurodevelopment in mice, accompanied by impaired neuronal maturation in the hippocampus and cortex, disrupted synaptic plasticity, and pronounced cognitive and behavioral abnormalities [12]. These findings suggest that *Mex3c* may be a potential candidate gene involved in the pathogenesis of NDDs. However, how *Mex3c* deficiency leads to hippocampal neuronal injury and which specific form of cell death mediates the associated neurobehavioral abnormalities remain unclear.

Ferroptosis is a form of regulated cell death driven by iron-dependent lipid peroxidation[13]. Its major biochemical features include dysregulated iron homeostasis, enhanced lipid peroxidation and oxidative stress, and impairment of cellular antioxidant defense systems[14]. Unlike other forms of cell death, ferroptosis is morphologically characterized at the ultrastructural level by shrunken mitochondria, increased mitochondrial membrane density, and reduced or absent mitochondrial cristae [15]. The central nervous system is enriched in polyunsaturated fatty acids and has a high oxidative metabolic demand,

rendering neurons particularly susceptible to iron-dependent lipid peroxidation[16]. Increasing evidence indicates that ferroptosis contributes to neuronal injury in various neurological disorders, including Alzheimer's disease, ischemic brain injury, and traumatic brain injury[17, 18]. In addition, recent studies have shown that brain injury during development is likewise accompanied by marked disturbances in iron metabolism and enhanced lipid peroxidation, whereas treatment with the ferroptosis inhibitor Ferrostatin-1 (Fer-1) can attenuate hippocampal neuronal injury and ameliorate associated cognitive and emotional abnormalities[19]. Ferroptosis-related pathological alterations, including cerebral iron accumulation, enhanced oxidative stress, and reduced antioxidant capacity, have also been observed in several models of NDDs[19].

Collectively, these findings suggest that aberrant activation of ferroptosis may represent an important pathological process linking genetic abnormalities to neuronal injury during development.

Glutathione peroxidase 4 (GPX4) is a key antioxidant enzyme that protects neurons against ferroptosis and serves as a central effector of the system Xc^-–GSH–GPX4 defense axis[20]. GPX4 uses reduced glutathione (GSH) to detoxify lipid hydroperoxides within cellular membranes, thereby suppressing lipid peroxidation chain reactions and maintaining cellular redox homeostasis [21]. When GPX4 expression or activity is reduced, the cellular capacity to eliminate lipid peroxides is compromised, resulting in the persistent accumulation of ROS and lipid peroxidation products and ultimately increasing cellular susceptibility to ferroptosis[21]. Meanwhile, ferritin metabolism mediated by ferritin heavy chain 1 (FTH1) and nuclear receptor coactivator 4 (NCOA4) also contributes to the regulation of intracellular labile iron levels and ferroptosis sensitivity. Notably, RNA-binding proteins have been shown to modulate ferroptosis-related molecules through post-transcriptional regulation or the control of protein homeostasis [22]. For example, members of the MEX3 family and other RNA-binding proteins can regulate the expression of ferroptosis-associated factors, including p53, GPX4, and SLC7A11[23]. Given that MEX3C possesses both RNA-binding activity and the ability to regulate protein homeostasis, whether MEX3C deficiency impairs GPX4-mediated antioxidant defense and subsequently induces ferroptosis in hippocampal neurons is an important question that remains to be systematically elucidated.

Against this background, the present study aimed to investigate the role and molecular mechanisms of MEX3C in neurodevelopment, with a particular focus on whether *Mex3c* deficiency causes neurodevelopmental impairment, whether the resulting abnormalities are associated with hippocampal neuronal injury and ferroptosis, and whether ferroptosis contributes to the NDD-like phenotypes induced by *Mex3c* deficiency. To address these questions, we established a MEX3C knockout mouse model to characterize neurodevelopmental and behavioral alterations and further investigated, at the molecular and cellular levels, the mechanisms through which *Mex3c* deficiency contributes to neurodevelopmental dysfunction.

2. Materials and Methods

2.1 Experimental Animals

Heterozygous *Mex3c*$^{+/-}$ mice on a C57BL/6J genetic background were purchased from Cyagen Biosciences (Guangdong, China; License No. SCXK [Guangdong] 2018-0032). Three-month-old specific-pathogen-free (SPF) male and female *Mex3c*$^{+/-}$ mice were intercrossed. Polymerase chain reaction (PCR) genotyping of the offspring yielded wild-type (*Mex3c*$^{+/+}$, WT), heterozygous (*Mex3c*$^{+/-}$, HE), and homozygous knockout (*Mex3c*$^{-/-}$, KO) mice. Wild-type (*Mex3c*$^{+/+}$) littermates served as controls for *Mex3c*$^{-/-}$ mice.

All animals were maintained in an SPF-grade animal facility under controlled environmental conditions (temperature: 25°C; 12 h light/12 h dark cycle) with ad libitum access to standard laboratory chow and water. Eight-week-old WT and KO mice were used for baseline behavioral, histological, and molecular biology assays. For the Ferrostatin-1 (Fer-1) intervention experiments, pharmacological administration commenced at 5 weeks of age and continued for 3 consecutive weeks; behavioral testing and tissue harvesting were subsequently performed at 8 weeks of age. All animal protocols complied strictly with the guidelines for the care and use of laboratory animals of Ningxia Medical University and were approved by the Animal Ethics Committee of Ningxia Medical University.

2.2 *Mex3c* Genotyping

Tail tips (~ 2 mm) were harvested from 3-week-old mice and placed into sterile microcentrifuge tubes. To each tube, 40 μL of Lysis Buffer A and 10 μL of Proteinase K were added. After thorough mixing, tissues were digested at 50°C for 10 min, followed by incubation at 95°C for 10 min to heat-inactivate Proteinase K. Samples were centrifuged at 12,000 × g for 3 min, and the resulting supernatant was collected as the DNA template for PCR amplification.

PCR amplification was performed using forward primer F in combination with reverse primers R1 and R2. Primer sequences were as follows: F: 5'-CTAGAACCAGAGATAATCCAGAG-3'

R1: 5'-CAGGAGTGTAAGTTAGAAAGGAG-3'

R2: 5'-TAGACCTCCCGCCTGGTTTAA-3'. The 20-μL PCR reaction mixture comprised 1 μL of DNA template, 0.5 μL of each forward and reverse primer, 10 μL of Mouse Direct PCR Mix, and nuclease-free water. The thermocycling parameters were as follows: initial denaturation at 94°C for 3 min; 35 cycles of denaturation at 94°C for 30 s, annealing at 62°C for 35 s, and extension at 72°C for 35 s; followed by a final extension at 72°C for 5 min. PCR products were separated on a 2% agarose gel by electrophoresis at 120 V for 40 min. Gel images were captured using a gel documentation system, and genotypes (WT, HE, and KO) were determined based on distinct band patterns. Genotypes of all experimental animals were independently reconfirmed before formal procedures.

2.3 Real-Time Quantitative PCR (RT-qPCR)

Total RNA was extracted from fresh hippocampal tissues of WT and KO mice using TRIzol reagent (Invitrogen, Cat. No. 15596026CN). RNA integrity was evaluated using an Agilent 2100 Bioanalyzer, and only samples satisfying the quality control criteria (RNA Integrity Number [RIN] meeting experimental standards) were selected for downstream analysis. Equal amounts of total RNA were reverse-transcribed into cDNA using PrimeScript RT Master Mix (TaKaRa, Cat. No. RR036Q).

Quantitative real-time PCR (RT-qPCR) was performed on a Bio-Rad Real-Time PCR System using Hieff UNICON Universal Blue qPCR SYBR Green Master Mix (Yeasen, Cat. No. 11201ES03). Gapdh was used as the internal reference gene. Each biological sample was run in technical triplicate. Relative mRNA expression levels of *Mex3c* were quantified using the $2^{-\Delta\Delta CT}$

method. The primer sequences used in this study were as follows:

Mex3c:

Forward (F): 5'-ATGCTGTCCCACGCCTAC-3'

Reverse (R): 5'-AGTGCTTTAATTTTACAACCCTGG-3'

Gapdh:

Forward (F): 5'-TGCACCACCAACTGCTTAG-3'

Reverse (R): 5'-GACGCAGGGATGATGTTC-3'

2.4 Fer-1 Treatment

Ferrostatin-1 (Fer-1; MedChemExpress, Cat. No. HY-100579) was dissolved in a vehicle consisting of 2% DMSO, 50% PEG300, 5% Tween 80, and double-distilled water (ddH_2O) to prepare a 5 mg/mL stock solution. Five-week-old *Mex3c*$^{-/-}$ mice (~ 20 g body weight) received daily intraperitoneal (i.p.) injections of Fer-1 (3 mg/kg/day) at a fixed time for 3 consecutive weeks. The general health and physical condition of the animals were closely monitored throughout the treatment period.

2.5 Behavioral Testing

All behavioral assays were conducted in a quiet environment with constant illumination. Mice were habituated to the testing room for at least 1 h before testing. Between individual trials, the testing apparatuses were thoroughly cleaned with 75% ethanol to eliminate olfactory cues. Animal movement trajectories and parameters were automatically recorded and analyzed using a video tracking system.

2.5.1 Open Field Test (OFT)

The open field apparatus comprised a 1×1 m square enclosure with a wall height of 30–50 cm. Each mouse was placed in the center of the arena and allowed to explore freely for 5 min. Locomotor

trajectories were recorded. The evaluated parameters included total distance traveled, percentage of time spent in the central area (%), and the number of entries into the central zone.

2.5.2 Light-Dark Box Test (LDB)

The LDB apparatus consisted of interconnected light and dark compartments. Mice were gently placed into the light chamber and allowed to explore the apparatus for 5 min. Time spent in the light box, total distance traveled, and the number of transitions between the light and dark compartments were recorded.

2.5.3 Novel Object Recognition (NOR) Test

The NOR test was conducted in three sequential phases: habituation, training, and testing. During habituation, mice explored an empty arena for 10 min. In the training phase, two identical objects were fixed in the arena, and mice were allowed to explore for 5 min. Following a 1-h inter-trial interval, one familiar object was replaced with a novel object of a different shape and color, and mice were re-introduced to explore for 5 min. The exploration time for familiar and novel objects (defined as the snout oriented toward the object within a distance of < 2 cm accompanied by sniffing behavior) was recorded.

2.6 Brain Tissue Harvesting and Paraffin Sectioning

Upon completion of behavioral testing, mice were deeply anesthetized with isoflurane and transcardially perfused via the left ventricle with ice-cold PBS followed by 4% paraformaldehyde (PFA). Whole brains were excised, post-fixed in 4% PFA at 4°C for 5 h, and washed with PBS. Samples were dehydrated through a graded ethanol series, cleared in xylene, and embedded in paraffin blocks. Coronal sections (2.5 μm thick) were cut and baked at 60°C for 2 h. Sections encompassing the hippocampal CA1, CA3, and dentate gyrus (DG) regions were selected for subsequent staining.

2.7 Nissl Staining

Paraffin sections were deparaffinized, rehydrated, and immersed in Nissl staining solution (Servicebio) for 5 min. After rinsing in water, sections were differentiated in a graded ethanol series, cleared in xylene, and mounted with neutral balsam. Low-magnification hippocampal images and high-magnification localized views of the CA1, CA3, and DG subregions were captured under a microscope. For each mouse, three non-overlapping fields per hippocampal subregion were randomly selected. Nissl-positive neurons and total cells were counted using ImageJ software. The percentage of Nissl-positive neurons was calculated as: (Nissl-positive cells/total cells)×100%.

2.8 NeuN Immunohistochemistry

Following deparaffinization and rehydration, sections were incubated in 3% H_2O_2 solution at room temperature in the dark for 10 min to block endogenous peroxidase activity. Heat-induced antigen retrieval was performed using EDTA buffer. Sections were blocked with goat serum for 30 min and subsequently incubated with a primary rabbit anti-NeuN monoclonal antibody (Abcam, Cat. No. ab177487, 1:800) at 4°C overnight. The following day, sections were incubated with an HRP-conjugated

secondary antibody, visualized with 3,3'-diaminobenzidine (DAB), counterstained with hematoxylin, dehydrated, cleared, and mounted. The percentage of NeuN-positive immunoreactive area (% area) in the hippocampal CA1, CA3, and DG subregions was quantified using ImageJ software.

2.9 GPX4 Immunofluorescence Staining

Following deparaffinization, rehydration, and antigen retrieval, sections were blocked with 5% normal goat serum for 30 min. Sections were then incubated with a primary rabbit anti-GPX4 monoclonal antibody (Abcam, Cat. No. ab125066, 1:100) overnight at 4°C in a humidified chamber. After washing with PBST, sections were incubated with an Alexa Fluor 594-conjugated goat anti-rabbit secondary antibody (Abcam, Cat. No. ab150080, 1:500) for 1 h at room temperature in the dark. Cell nuclei were counterstained with DAPI, and sections were mounted with an anti-fade mounting medium. Images were acquired under a fluorescence microscope, and the mean fluorescence intensity (MFI) of GPX4 in each hippocampal subregion was quantified.

2.10 Western Blotting

Total protein was extracted from fresh hippocampal tissues, and protein concentrations were determined using a BCA protein assay kit. Equal amounts of protein (40 μg) were separated by SDS-PAGE and transferred onto PVDF membranes using a wet transfer system (300 mA, 1 h). Membranes were blocked with quick-blocking buffer for 10 min and incubated overnight at 4°C with primary antibodies against GPX4 (CST, Cat. No. 52455, 1:1,000), FTH1 (Abcam, Cat. No. ab183781, 1:1,000), NCOA4 (Proteintech, Cat. No. 83394-4-RR, 1:2,000), and GAPDH (Servicebio, Cat. No. GB15002, 1:5,000). After washing with PBST, membranes were incubated with HRP-conjugated secondary antibodies for 1 h at room temperature and visualized using enhanced chemiluminescence (ECL) reagents. Band densities were quantified using ImageJ software and normalized to GAPDH as the loading control.

2.11 Measurement of Reactive Oxygen Species (ROS) Levels

Fresh hippocampal tissues were minced and digested with an enzymatic digestion solution at 37°C for 20–30 min. The digest was filtered through a 300-mesh nylon mesh to prepare a single-cell suspension. After centrifugation and resuspension, cells were incubated with 10 μM DCFH-DA probe at 37°C for 1 h in the dark. After washing to remove extracellular probes, fluorescence intensity was measured using a microplate reader at an excitation wavelength of 488 nm and an emission wavelength of 525 nm. ROS levels were expressed as relative fluorescence intensity (RFI).

2.12 Determination of Reduced Glutathione (GSH) Content

Reduced glutathione (GSH) levels were quantified using a GSH Assay Kit (Solarbio, Cat. No. BC1175) according to the manufacturer's protocol. Hippocampal tissues were homogenized on ice and centrifuged to collect the supernatant. Absorbance was measured at 412 nm using the DTNB colorimetric method. GSH concentration was calculated from a standard curve and normalized to total protein concentration (μg/g protein).

2.13 Determination of Malondialdehyde (MDA) Content

Malondialdehyde (MDA) levels were measured using an MDA Assay Kit (Solarbio, Cat. No. BC0025) following the manufacturer's instructions. Hippocampal tissue homogenates were centrifuged, and the supernatant was mixed with the MDA working solution and boiled in a 100°C water bath for 60 min. After cooling in an ice bath and centrifuging, absorbances were measured at 532 nm and 600 nm. The MDA content was calculated and expressed as nmol/g protein.

2.14 Statistical Analysis

Statistical analyses and graphical illustrations were performed using GraphPad Prism 9.0 software. Data are presented as mean ± standard deviation (Mean ± SD), with each n value representing an independent experimental animal. Comparisons between two groups were analyzed using an unpaired two-tailed Student's t-test. Comparisons among three groups were analyzed using one-way analysis of variance (ANOVA) followed by Tukey's post hoc multiple comparisons test. A value of $p < 0.05$ was considered statistically significant (* $p < 0.05$, ** $p < 0.01$, *** $p < 0.001$, **** $p < 0.0001$; ns, non-significant).

3.Results

3.1 Validation of the *Mex3c* Knockout Mouse Model and Neurobehavioral Phenotypic Analysis

Heterozygous *Mex3c*$^{+/-}$ mice were intercrossed to generate homozygous *Mex3c*$^{-/-}$ knockout (KO) mice and wild-type *Mex3c*$^{+/+}$ (WT) littermate controls. To validate the knockout efficiency, mouse genotypes and hippocampal *Mex3c* expression levels were evaluated. Agarose gel electrophoresis of PCR amplification products revealed distinct band patterns consistent with the expected genotypes of WT, HE, and KO mice (Fig. 1A). Subsequent RT-qPCR analysis demonstrated that *Mex3c* mRNA expression in the hippocampus of KO mice was significantly reduced compared with that in WT controls, confirming successful gene ablation (Fig. 1B).

The open field test (OFT), light-dark box (LDB) test, and novel object recognition (NOR) test were subsequently performed to assess the impact of *Mex3c* deficiency on behavioral phenotypes. In the OFT, no significant difference was observed in total distance traveled between WT and KO mice (Fig. 1C, D). However, compared with WT mice, KO mice displayed a significantly lower percentage of time spent in the central area and fewer entries into the central zone (Fig. 1E, F). In the LDB test, KO mice exhibited markedly reduced time spent in the light box, shorter distance traveled within the light chamber, and fewer transitions between the light and dark compartments relative to WT controls (Fig. 1G–J). In the NOR test, both the recognition index and discrimination index were significantly decreased in KO mice (Fig. 1K–M).

Taken together, these results indicate that *Mex3c* deficiency does not overtly alter overall locomotor activity in the open field, but significantly reduces exploratory behavior in both the central zone and light chamber while impairing novel object recognition. These findings demonstrate that loss of *Mex3c* precipitates heightened anxiety-like behaviors and recognition memory deficits in mice.

3.2 *Mex3c* Deficiency Impairs Hippocampal Neuronal Integrity and Reduces NeuN Immunoreactivity in Mice

To evaluate the impact of *Mex3c* deficiency on hippocampal neurons, Nissl staining and NeuN immunohistochemical (IHC) staining were performed on hippocampal sections from WT and KO mice. Nissl staining revealed that, compared with WT controls, KO mice exhibited loosely arranged neuronal layers, diminished staining intensity, and a significantly reduced proportion of Nissl-positive neurons in the hippocampal CA1, CA3, and dentate gyrus (DG) subregions (Fig. 2A–D).

Consistent with the Nissl staining findings, NeuN IHC staining demonstrated markedly weaker immunoreactive signals across the CA1, CA3, and DG regions in KO mice than in WT mice. Quantitative analysis further confirmed that the percentage of NeuN-positive immunoreactive area was significantly decreased in all three hippocampal subregions of KO mice (Fig. 2E–H).

Taken together, these findings demonstrate that loss of *Mex3c* leads to a marked reduction in both Nissl-positive cell counts and NeuN immunoreactivity across the hippocampal CA1, CA3, and DG subregions, indicating that *Mex3c* deficiency severely impairs hippocampal neuronal integrity.

1. (A) Representative images of Nissl staining in hippocampal tissues from WT and KO mice. Rectangular boxes denote the CA1, CA3, and dentate gyrus (DG) subregions, with high-magnification views of the corresponding areas shown on the right. Scale bars: low-magnification images, 100 μm; high-magnification images, 20 μm. (B–D) Quantitative analysis of the percentage of Nissl-positive cells in the hippocampal CA1, CA3, and DG subregions. (E) Representative images of NeuN immunohistochemical staining in hippocampal tissues from WT and KO mice. Rectangular boxes denote the CA1, CA3, and DG subregions, with high-magnification views of the corresponding areas shown on the right. Scale bars: low-magnification images, 100 μm; high-magnification images, 20 μm. (F–H) Quantitative analysis of the percentage of NeuN-positive immunoreactive area in the hippocampal CA1, CA3, and DG subregions. Data are expressed as mean ± SD (n = 6 mice/group). Comparisons between two groups were analyzed using an unpaired two-tailed Student's t-test. *$P < 0.05$; **$P < 0.01$.

1. **3.3 Mex3c Deficiency Induces GPX4 and FTH1 Downregulation, NCOA4 Upregulation, and Redox Imbalance in the Mouse Hippocampus**

To evaluate the impact of *Mex3c* deficiency on hippocampal ferroptotic status, GPX4 expression across hippocampal subregions, ferroptosis-associated protein levels, and redox parameters were analyzed. Immunofluorescence staining revealed that the mean fluorescence intensity (MFI) of GPX4 was

significantly decreased in the CA1, CA3, and dentate gyrus (DG) subregions of KO mice compared with WT controls (Fig. 3A–D).

Consistent with these observations, Western blot analysis demonstrated significant downregulation of GPX4 and FTH1 protein expression, along with marked upregulation of NCOA4 protein levels in the hippocampal tissues of KO mice relative to WT controls (Fig. 3E–H). Biochemical assays further revealed profound redox dyshomeostasis in the hippocampus of KO mice, as evidenced by significant elevations in ROS and MDA levels alongside a substantial depletion of GSH content (Fig. 3I–K).

Taken together, these findings demonstrate that *Mex3c* loss impairs the GPX4-mediated antioxidant defense system in the hippocampus, accompanied by FTH1 suppression, NCOA4 induction, ROS and MDA accumulation, and GSH depletion. These data indicate that *Mex3c* deficiency triggers ferroptotic stress in hippocampal tissue.

1. (A) Representative immunofluorescence images of GPX4 in the hippocampal CA1, CA3, and dentate gyrus (DG) subregions of WT and KO mice. GPX4 is stained in red, and cell nuclei are counterstained with DAPI in blue. High-magnification views of the white boxed regions are shown on the right. Scale bars: low-magnification images, 500 μm; high-magnification images, 100 μm. (B–D) Quantitative analysis of the mean fluorescence intensity (MFI) of GPX4 in the hippocampal CA1, CA3, and DG subregions. (E) Representative Western blot images showing protein expression of FTH1, NCOA4, and GPX4 in hippocampal tissues of WT and KO mice, with GAPDH as the loading control. (F–H) Quantitative analysis of relative protein expression levels of FTH1, GPX4, and NCOA4. (I–K) Quantitative analysis of ROS levels, MDA content, and GSH content in hippocampal tissues of WT and KO mice. Data are expressed as mean ± SD (n = 6 mice/group). Comparisons between two groups were analyzed using an unpaired two-tailed Student's t-test. *$P < 0.05$; **$P < 0.01$; ***$P < 0.001$; ****$P < 0.0001$.

1. **3.4 Fer-1 Treatment Partially Restores Hippocampal GPX4 and FTH1 Expression and Alleviates Redox Dyshomeostasis in Mex3c-Deficient Mice**

To verify whether ferroptotic stress contributes to hippocampal abnormalities induced by *Mex3c* deficiency, *Mex3c* KO mice were treated with the specific ferroptosis inhibitor Ferrostatin-1 (Fer-1), followed by the assessment of hippocampal GPX4, FTH1, and redox parameters. Immunofluorescence analysis demonstrated that the mean fluorescence intensity (MFI) of GPX4 was significantly decreased in the CA1, CA3, and dentate gyrus (DG) subregions of KO mice compared with WT controls. Notably, Fer-1 treatment (KO + Fer-1 group) significantly increased GPX4 MFI across all three subregions compared with untreated KO mice, although levels remained lower than those in WT controls (Fig. 4A–D).

Biochemical assays revealed that ROS and MDA levels were significantly elevated, while GSH content was markedly depleted, in hippocampal tissues of KO mice relative to WT controls. Compared with the untreated KO group, Fer-1 administration significantly attenuated ROS and MDA levels while increasing

GSH content (Fig. 4E, F, I). Consistent with these biochemical changes, Western blot analysis confirmed that FTH1 protein expression in the hippocampus was significantly lower in KO mice than in WT controls, whereas Fer-1 intervention markedly upregulated FTH1 protein levels in KO mice (Fig. 4G, H).

Taken together, these results demonstrate that Fer-1 intervention partially restores GPX4 and FTH1 expression, dampens ROS and MDA accumulation, and alleviates GSH depletion in the hippocampus of *Mex3c*-deficient mice. These findings support the causative involvement of ferroptotic stress in *Mex3c* loss-induced hippocampal redox dyshomeostasis.

1. (A) Representative immunofluorescence images of GPX4 in the hippocampal CA1, CA3, and dentate gyrus (DG) subregions of WT, KO, and KO + Fer-1 mice. GPX4 is stained in red, and cell nuclei are counterstained with DAPI in blue. High-magnification views of the white boxed regions are shown on the right. Scale bars: low-magnification images, 10 μm; high-magnification images, 20 μm. (B–D) Quantitative analysis of the mean fluorescence intensity (MFI) of GPX4 in the hippocampal CA1, CA3, and DG subregions. (E) Quantitative analysis of ROS levels in hippocampal tissues across groups. (F) Quantitative analysis of MDA content in hippocampal tissues across groups. (G) Representative Western blot images showing FTH1 protein expression in hippocampal tissues across groups, with GAPDH as the loading control. (H) Quantitative analysis of relative FTH1 protein expression levels. (I) Quantitative analysis of GSH content in hippocampal tissues across groups. Data are expressed as mean ± SD (n = 3 independent biological replicates/group). Comparisons among three groups were analyzed using one-way ANOVA followed by Tukey's post hoc multiple comparisons test. **P* < 0.05; ***P* < 0.01; ****P* < 0.001; *****P* < 0.0001.

1. **3.5 Fer-1 Treatment Ameliorates Hippocampal NeuN Immunoreactivity and Rescues Recognition Memory and Anxiety-like Behaviors in Mex3c-Deficient Mice**

To further evaluate the effects of Fer-1 treatment on hippocampal neuronal integrity and neurobehavioral phenotypes in *Mex3c*-deficient mice, NeuN immunohistochemistry, the novel object recognition (NOR) test, and the light-dark box (LDB) test were conducted in WT, KO, and KO + Fer-1 mice.

NeuN immunohistochemistry demonstrated that, compared with WT controls, the percentage of NeuN-positive immunoreactive area across the hippocampal CA1, CA3, and dentate gyrus (DG) subregions was significantly reduced in KO mice. Notably, compared with the untreated KO group, Fer-1 administration (KO + Fer-1 group) significantly increased NeuN immunoreactivity across all three subregions, although levels did not fully recover to those of the WT group (Fig. 5A–D).

In the NOR test, both the recognition index and discrimination index were markedly lower in KO mice than in WT controls. Following Fer-1 intervention, both the recognition and discrimination indices were significantly higher in the KO + Fer-1 group than in the untreated KO group, indicating that Fer-1 administration substantially improved recognition memory in *Mex3c*-deficient mice (Fig. 5E–G).

In the LDB test, KO mice spent significantly less time, traveled shorter distances in the light compartment, and exhibited fewer transitions between the light and dark chambers compared with WT controls. Relative to the untreated KO group, Fer-1 treatment significantly increased time spent and distance traveled in the light chamber, as well as the frequency of transitions between compartments (Fig. 5H–K).

Taken together, these results demonstrate that Fer-1 intervention partially restores hippocampal NeuN immunoreactivity and rescues recognition memory deficits and anxiety-like behaviors, further supporting the causative role of ferroptotic stress in *Mex3c* deficiency-induced hippocampal neuronal damage and neurobehavioral impairments.

(A) Representative images of NeuN immunohistochemical staining in hippocampal tissues from WT, KO, and KO + Fer-1 mice. Rectangular boxes denote the CA1, CA3, and dentate gyrus (DG) subregions, with high-magnification views of the corresponding areas shown on the right. Scale bars: low-magnification images, 100 μm; high-magnification images, 20 μm. (B–D) Quantitative analysis of the percentage of NeuN-positive immunoreactive area in the hippocampal CA1, CA3, and DG subregions. (E) Representative locomotor trajectories and activity heatmaps of mice across groups in the novel object recognition (NOR) test. (F) Recognition index in the NOR test. (G) Discrimination index in the NOR test. (H) Representative locomotor trajectories and 3D activity heatmaps of mice across groups in the light-dark box (LDB) test. (I) Time spent in the light compartment. (J) Distance traveled within the light compartment. (K) Number of transitions between light and dark compartments. Data are expressed as mean ± SD (n = 6 mice/group). Comparisons among three groups were analyzed using one-way ANOVA followed by Tukey's post hoc multiple comparisons test. *$P < 0.05$; **$P < 0.01$; ***$P < 0.001$; ****$P < 0.0001$.

4. Discussion

This study investigated the effects of *Mex3c* deficiency on neurobehavioral phenotypes and hippocampal neuronal injury in mice and explored the potential underlying mechanisms. *Mex3c* knockout (KO) mice exhibited marked anxiety-like behavior and impaired recognition memory, accompanied by reduced neuronal integrity in the CA1, CA3, and dentate gyrus (DG) regions of the hippocampus. Further analysis showed that *Mex3c* deficiency decreased hippocampal GPX4 and FTH1 expression and increased NCOA4 expression, together with GSH depletion and accumulation of ROS and MDA. Notably, treatment with the ferroptosis inhibitor Ferrostatin-1 (Fer-1) alleviated these redox abnormalities and partially restored hippocampal neuronal status and behavioral phenotypes. These findings suggest that *Mex3c* deficiency may contribute to hippocampal neuronal injury and neurobehavioral abnormalities by impairing GPX4-related antioxidant defense and promoting ferroptosis-related damage.

Behavioral analysis showed that *Mex3c* KO mice displayed reduced exploration of the central area in the open field test, whereas the total distance traveled was unchanged, suggesting that the behavioral

alteration was more likely related to increased anxiety rather than impaired basal locomotor activity. Consistently, KO mice showed reduced exploration of the light compartment in the light-dark box test and lower recognition and discrimination indices in the novel object recognition test, indicating that *Mex3c* deficiency affects both anxiety-related behavior and recognition memory. These findings are generally consistent with previous studies implicating *Mex3c* in neurodevelopment and cognitive function[24]. Previous studies have shown that *Mex3c* is expressed in brain tissue and is involved in neurodevelopment, energy metabolism, and cellular homeostasis, whereas *Mex3c* deficiency can lead to cognitive impairment and neuronal injury [12]. In the present study, the proportion of Nissl-positive cells and NeuN-positive signals in the CA1, CA3, and DG regions of the hippocampus was markedly reduced in *Mex3c* KO mice, suggesting impaired hippocampal neuronal integrity. The hippocampus is a key brain region involved in learning, memory, and emotional regulation, and structural and functional abnormalities of the hippocampus have been reported in various neurodevelopmental disorders[25, 26]. Therefore, hippocampal neuronal injury induced by *Mex3c* deficiency may contribute to the observed anxiety-like behavior and recognition memory impairment.

Further analysis showed that hippocampal neuronal abnormalities caused by *Mex3c* deficiency were accompanied by a series of ferroptosis-related molecular and biochemical changes. Ferroptosis is a form of regulated cell death characterized primarily by iron-dependent lipid peroxidation and is closely associated with disrupted iron homeostasis, impaired antioxidant capacity, and lipid peroxide accumulation[27]. In this study, hippocampal ROS and MDA levels were significantly increased, whereas GSH levels were decreased in *Mex3c* KO mice, indicating disrupted redox homeostasis and enhanced lipid peroxidation. In addition, FTH1 expression was decreased, and NCOA4 expression was increased in KO mice. FTH1 participates in intracellular iron storage and limits free iron-mediated oxidative damage[28], whereas NCOA4 mediates ferritinophagy and promotes the release of stored iron[29]. Thus, reduced FTH1 and increased NCOA4 may reflect altered ferritin metabolism and iron homeostasis after *Mex3c* deficiency and may increase neuronal susceptibility to iron-dependent lipid peroxidation. Together with GSH depletion and enhanced lipid peroxidation, these findings suggest that ferroptosis-related damage may be involved in hippocampal neuronal abnormalities induced by *Mex3c* deficiency.

GPX4 is a key antioxidant enzyme that suppresses ferroptosis [30]by using GSH to reduce membrane phospholipid hydroperoxides and thereby interrupt lipid peroxidation chain reactions [21, 31]. In this study, GPX4 signals were markedly reduced in the CA1, CA3, and DG regions of the hippocampus in *Mex3c* KO mice. Western blot analysis further confirmed reduced hippocampal GPX4 protein expression, accompanied by decreased GSH and increased ROS and MDA levels, suggesting that *Mex3c* deficiency may impair GPX4-related antioxidant defense. More importantly, Fer-1 treatment reduced hippocampal ROS and MDA levels, increased GSH levels, and partially restored GPX4 and FTH1 expression in KO mice. Fer-1 also improved NeuN-positive signals as well as anxiety-like behavior and recognition memory deficits. Fer-1 is a classical ferroptosis inhibitor that scavenges lipid radicals and suppresses lipid peroxidation chain reactions[32, 33]. Therefore, the concurrent improvement in ferroptosis-related biochemical changes, neuronal injury, and behavioral abnormalities after Fer-1 treatment provides further

pharmacological evidence for the involvement of ferroptosis in the phenotype caused by *Mex3c* deficiency. Previous studies have shown that ferroptosis contributes to neuronal injury in various neurological disorders[16, 34, 35], and abnormalities in ferroptosis-related pathways, including SLC7A11/GPX4, have also been reported in some ASD-related animal models [36]. The present findings further suggest that *Mex3c* deficiency may impair GPX4-related antioxidant defense, thereby increasing the susceptibility of hippocampal neurons to lipid peroxidation and ferroptosis-related injury and ultimately contributing to neurobehavioral abnormalities.

MEX3C has both RNA-binding and E3 ubiquitin ligase-related functions, suggesting that it may participate in these processes through post-transcriptional regulation or protein homeostasis[8, 37]. Previous studies have shown that RNA-binding proteins can influence cellular susceptibility to ferroptosis by regulating the RNA processing, stability, or expression of ferroptosis-related molecules [38, 39]. Therefore, the reduction in GPX4 expression following *Mex3c* deficiency suggests a potential regulatory relationship between MEX3C and GPX4. However, this study did not directly demonstrate an interaction between MEX3C and Gpx4 mRNA or GPX4 protein, and it therefore remains unclear whether MEX3C directly regulates GPX4. In addition, although Fer-1 markedly improved the molecular, neuronal, and behavioral phenotypes of KO mice, some parameters were not fully restored to WT levels. This suggests that ferroptosis-related injury may be one important mechanism underlying neurodevelopmental abnormalities caused by *Mex3c* deficiency, but is unlikely to be the only mechanism. Together with previous evidence that *Mex3c* is involved in neuronal maturation, synaptic plasticity, energy metabolism, and autophagic regulation, its deficiency may affect neuronal function through multiple interconnected cellular processes.

This study has several limitations. First, the assessment of ferroptosis was mainly based on GPX4, FTH1, NCOA4, ROS, MDA, and GSH, together with the pharmacological effects of Fer-1. Evidence from Fe^{2+} levels, lipid ROS, ACSL4, and ferroptosis-associated mitochondrial ultrastructure is still lacking. Therefore, the current results more directly support the presence of ferroptosis-related injury in hippocampal neurons following *Mex3c* deficiency, whereas whether *Mex3c* deficiency induces typical ferroptosis requires further verification. Second, the specific molecular mechanism by which MEX3C regulates GPX4 remains unclear. Future studies using RNA immunoprecipitation, Gpx4 mRNA stability assays, protein half-life measurements, and ubiquitination assays may help determine whether the RNA-binding and E3 ubiquitin ligase functions of MEX3C are involved in GPX4 regulation. In addition, Fer-1 represents a pharmacological intervention, and further studies using genetic manipulation of key molecules such as GPX4 or NCOA4 are needed to validate this mechanism. Finally, this study mainly examined endpoint changes in the hippocampus of 8-week-old mice. The temporal sequence among *Mex3c* deficiency, ferroptosis-related abnormalities, neuronal injury, and behavioral phenotypes remains to be clarified through longitudinal analyses at different developmental stages.

In conclusion, *Mex3c* deficiency induces anxiety-like behavior and recognition memory impairment in mice and is accompanied by hippocampal neuronal injury. *Mex3c* deficiency is also associated with

impaired GPX4-related antioxidant defense, alterations in iron homeostasis-related proteins, and enhanced lipid peroxidation, whereas Fer-1 partially reverses these molecular, neuronal, and behavioral changes. These findings suggest that impaired GPX4-related antioxidant defense and ferroptosis-related injury may represent important mechanisms contributing to hippocampal neuronal damage and neurobehavioral abnormalities caused by *Mex3c* deficiency, providing further experimental evidence for understanding the role of *Mex3c* in neurodevelopmental disorders.

Declarations

Conflict of interest

The authors declare that the research was conducted in the absence of any commercial or financial relationships that could be construed as a potential conflict of interest.

Generative AI statement

The authors declare that no Generative AI was used in the creation of this manuscript.

Funding

Author Contribution

HC: Conceptualization, Data curation, Formal analysis, Investigation, Methodology, Project administration, Resources, Software, Supervision, Validation, Visualization, Writing – original draft, Writing – review & editing.DL: Conceptualization, Methodology, Project administration, Resources,Writing – review & editing.ZCD: Data curation, Formal analysis, Investigation, Methodology, Software, Validation, Visualization, Writing – review & editing.ZLS:Investigation, Methodology,Visualization, Supervision, Project administration, Writing – review & editing.LHM: Formal analysis, Investigation,Funding acquisition, Methodology, Resources, Supervision, Validation, Visualization, Writing – review & editing.YD: Funding acquisition, Investigation, Methodology, Project administration, Resources, Software, Validation, Visualization, Writing – review & editing.

Data availability statement

The authors do not have permission to share data.

Ethics statement

The animal study was approved by the Ethics Review Committee of the General Hospital of Ningxia Medical University for Medical Scientific Research. The study was conducted in accordance with the local legislation and institutional requirements.

The author(s) declare that financial support was received for the research and/or publication of this article. This research wasfunded by the National Natural Science Foundation of China, grant number 82260308.

References

1. MARTíNEZ DE, LAGRáN M, BASCóN-CARDOZO K (2024) Neurodevelopmental disorders: 2024 update [J]. Free Neuropathol 5:20
2. TAFOLLA M, SINGER H (2025) Autism Spectrum Disorder Across the Lifespan [J]. Annu Rev Clin Psychol 21(1):193–220
3. EIGSTI I M (2024) The Autism Constellation and Neurodiversity: Long-Term and Adult Outcomes in Autism Spectrum Disorder [J]. Pediatr Clin North Am 71(2):327–341
4. GAO S, SHAN C, ZHANG R et al (2021) Genetic advances in neurodevelopmental disorders [J]. Med Rev 2025, 5(2): 139 – 51
5. LEBLOND C S, ROLLAND T (2024) A Genetic Bridge Between Medicine and Neurodiversity for Autism [J]. Annu Rev Genet 58(1):487–512
6. CORTESE S, BELLATO A, GABELLONE A et al (2025) Latest clinical frontiers related to autism diagnostic strategies [J]. Cell Rep Med 6(2):101916
7. BUCHET-POYAU K, COURCHET J, LE HIR H et al (2007) Identification and characterization of human Mex-3 proteins, a novel family of evolutionarily conserved RNA-binding proteins differentially localized to processing bodies [J]. Nucleic Acids Res 35(4):1289–1300
8. YANG L, WANG C, LI F et al (2017) The human RNA-binding protein and E3 ligase MEX-3C binds the MEX-3-recognition element (MRE) motif with high affinity [J]. J Biol Chem 292(39):16221–16234
9. LI T, QIN J, HUANG Z et al (2026) A DNA Aptamer as a Chemical Tool to Modulate MEX3C-Mediated mRNA Destabilization [J]. ACS Appl Bio Mater 9(3):1643–1654
10. JIAO Y, GEORGE S K, ZHAO Q et al (2012) Mex3c mutation reduces adiposity and increases energy expenditure [J]. Mol Cell Biol 32(21):4350–4362
11. JIAO Y, BISHOP C E, LU B (2012) Mex3c regulates insulin-like growth factor 1 (IGF1) expression and promotes postnatal growth [J]. Mol Biol Cell 23(8):1404–1413
12. CAI H, ZHANG C, ZHANG H et al (2025) Deletion of Mex3c gene leads to autistic-like behavior in mice by inhibiting AMPK signal pathway [J]. Front Behav Neurosci 19:1551440
13. DIXON S J, OLZMANN JA (2024) The cell biology of ferroptosis [J]. Nat Rev Mol Cell Biol 25(6):424–442

14. JIANG X, STOCKWELL B R CONRADM (2021) Ferroptosis: mechanisms, biology and role in disease [J]. Nat Rev Mol Cell Biol 22(4):266–282
15. THI NGHIEM T H, KUSUMA F, PARK J et al (2025) Brief guide to detecting ferroptosis [J]. Mol Cells 48(11):100276
16. JACQUEMYN J, RALHAN I, IOANNOU MS (2024) Driving factors of neuronal ferroptosis [J]. Trends Cell Biol 34(7):535–546
17. SHEN L, LIN D, LI X et al (2020) Ferroptosis in Acute Central Nervous System Injuries: The Future Direction? [J]. Front Cell Dev Biol 8:594
18. FENG L, SUN J (2024) Ferroptosis mechanism and Alzheimer's disease [J]. Neural Regen Res 19(8):1741–1750
19. LI C, WU Z, XUE H et al (2022) Ferroptosis contributes to hypoxic-ischemic brain injury in neonatal rats: Role of the SIRT1/Nrf2/GPx4 signaling pathway [J]. CNS Neurosci Ther 28(12):2268–2280
20. XIE Y, KANG R, KLIONSKY D J et al (2023) GPX4 in cell death, autophagy, and disease [J]. Autophagy 19(10):2621–2638
21. LIU Y, WAN Y, JIANG Y et al (2023) GPX4: The hub of lipid oxidation, ferroptosis, disease and treatment [J]. Biochim Biophys Acta Rev Cancer 1878(3):188890
22. CHEN X (2026) Decoding GPX4 regulation in ferroptosis: mechanisms and therapeutic implications [J]. Trends Mol Med 32(8):792–809
23. WANG C K, CHEN T J, TAN G Y T et al (2023) MEX3A Mediates p53 Degradation to Suppress Ferroptosis and Facilitate Ovarian Cancer Tumorigenesis [J]. Cancer Res 83(2):251–263
24. WANG K, ZHANG H N, DU Y (2023) MEX3C induces cognitive impairment in mice through autophagy inhibition [J]. Brain Behav 13(11):e3245
25. WHITE T A, MILLER S L, SUTHERLAND A E et al (2024) Perinatal compromise affects development, form, and function of the hippocampus part one; clinical studies [J]. Pediatr Res 95(7):1698–1708
26. LONG J, LI H, LIU Y et al (2024) Insights into the structure and function of the hippocampus: implications for the pathophysiology and treatment of autism spectrum disorder [J]. Front Psychiatry 15:1364858
27. RU Q, LI Y, CHEN L et al (2024) Iron homeostasis and ferroptosis in human diseases: mechanisms and therapeutic prospects [J]. Signal Transduct Target Ther 9(1):271
28. ZHANG DD (2024) Ironing out the details of ferroptosis [J]. Nat Cell Biol 26(9):1386–1393
29. HOELZGEN F, NGUYEN T T P KLUKINE et al (2024) Structural basis for the intracellular regulation of ferritin degradation [J]. Nat Commun 15(1):3802
30. HAMBRIGHT W S CHENL, NA R et al (2015) Ablation of the Ferroptosis Inhibitor Glutathione Peroxidase 4 in Neurons Results in Rapid Motor Neuron Degeneration and Paralysis [J]. J Biol Chem 290(47):28097–28106
31. URSINI F, BOSELLO TRAVAIN V, COZZA G et al (2022) A white paper on Phospholipid Hydroperoxide Glutathione Peroxidase (GPx4) forty years later [J]. Free Radic Biol Med 188:117–133

32. ZILKA O, SHAH R, LI B et al (2017) On the Mechanism of Cytoprotection by Ferrostatin-1 and Liproxstatin-1 and the Role of Lipid Peroxidation in Ferroptotic Cell Death [J]. ACS Cent Sci 3(3):232–243
33. MIOTTO G, ROSSETTO M, DI PAOLO M L et al (2020) Insight into the mechanism of ferroptosis inhibition by ferrostatin-1 [J]. Redox Biol 28:101328
34. ZHANG T, ZHANG Y, XIE J et al (2025) Ferroptosis in neurodegenerative diseases: mechanisms and therapeutic potential of stem cell derivatives [J]. Front Cell Dev Biol 13:1577382
35. WANG D, WU Y, ZHOU X et al (2024) Cadmium exposure induced neuronal ferroptosis and cognitive deficits via the mtROS-ferritinophagy pathway [J]. Environ Pollut 349:123958
36. JIANG P, ZHOU L, ZHAO L et al (2024) Puerarin attenuates valproate-induced features of ASD in male mice via regulating Slc7a11-dependent ferroptosis [J]. Neuropsychopharmacology 49(3):497–507
37. HE Z, ZHANG H (2024) Ubiquitylation of RUNX3 by RNA-binding ubiquitin ligase MEX3C promotes tumorigenesis in lung adenocarcinoma [J]. J Transl Med 22(1):216
38. XIE Y, LI Y, XIE Y et al (2025) CIRBP Stabilizes Slc7a11 mRNA to Sustain the SLC7A11/GPX4 Antioxidant Axis and Limit Ferroptosis in Doxorubicin-Induced Cardiotoxicity [J]. Antioxid (Basel), 14(8)
39. CHEN Y, ZHAO T, CHEN H et al (2025) RNA binding protein ALYREF regulates ferroptosis to facilitate LUAD growth and metastasis via promoting SLC7A11 mRNA stability [J]. Sci Rep 15(1):1351

Figures

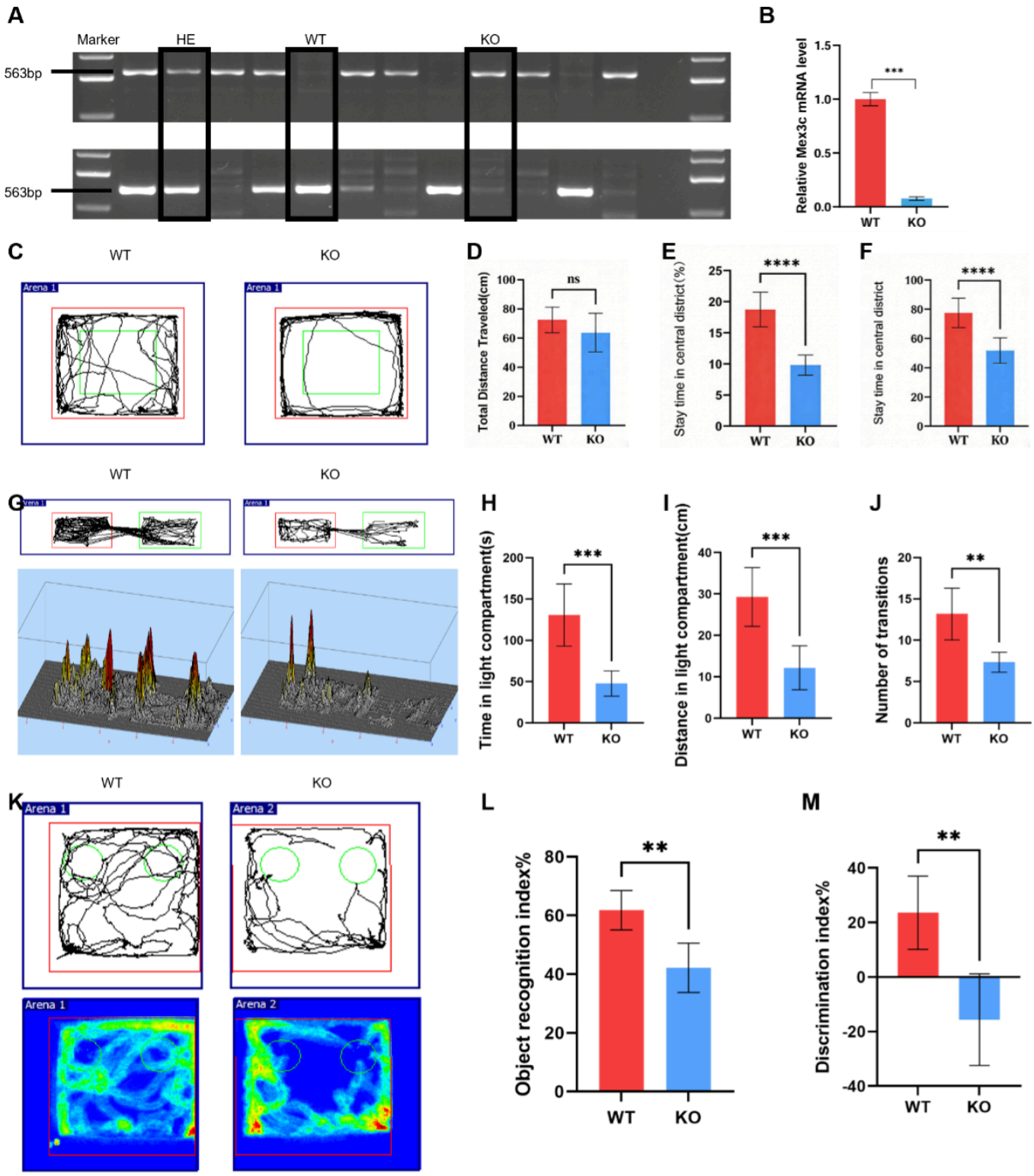


Figure 1

Validation of the *Mex3c* knockout mouse model and behavioral phenotypic analysis. (A) Representative agarose gel electrophoresis image of PCR genotyping for *Mex3c*$^{+/+}$ wild-type (WT), *Mex3c*$^{+/-}$ heterozygous (HE), and *Mex3c*$^{-/-}$ homozygous knockout (KO) mice. (B) Relative mRNA expression levels of *Mex3c* in hippocampal tissues of WT and KO mice measured by qRT-PCR. (C) Representative locomotor trajectories of WT and KO mice in the open field test (OFT). (D) Quantification of total

distance traveled in the OFT. (E) Percentage of time spent in the central zone. (F) Number of entries into the central zone. (G) Representative locomotor trajectories and 3D activity heatmaps of WT and KO mice in the light-dark box (LDB) test. (H) Time spent in the light compartment. (I) Distance traveled within the light compartment. (J) Number of transitions between light and dark compartments. (K) Representative locomotor trajectories and activity heatmaps of WT and KO mice in the novel object recognition (NOR) test. (L) Recognition index in the NOR test. (M) Discrimination index in the NOR test. Data are expressed as mean ± SD (n=6 mice/group). Comparisons between two groups were analyzed using an unpaired two-tailed Student's t-test. ns, non-significant; *P < 0.05; **P < 0.01; *** P < 0.001; **** P < 0.0001.

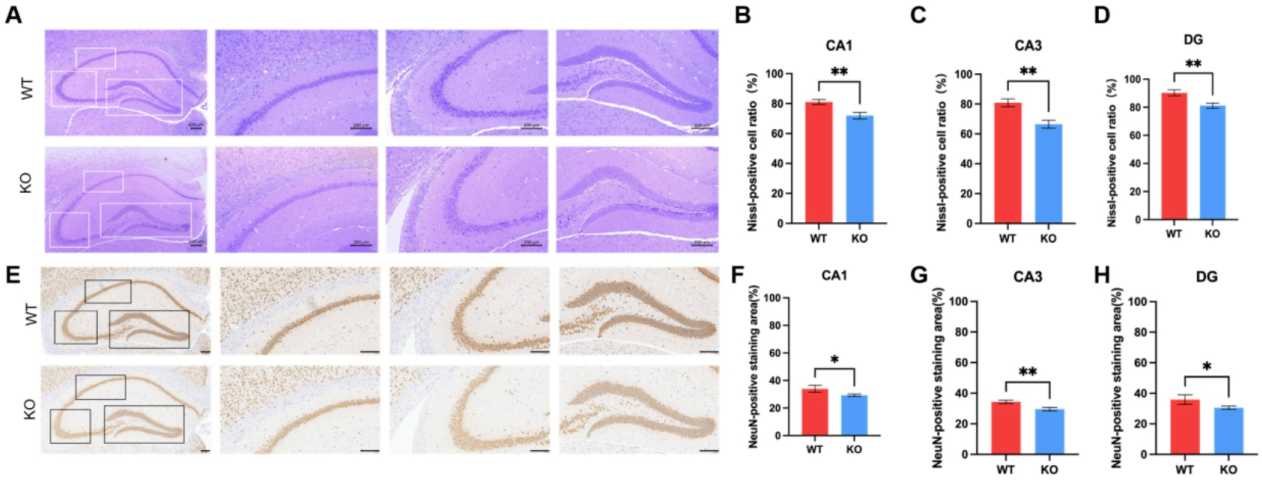


Figure 2

Effects of *Mex3c* deficiency on hippocampal neuronal integrity and NeuN immunoreactivity in mice.

(A) Representative images of Nissl staining in hippocampal tissues from WT and KO mice. Rectangular boxes denote the CA1, CA3, and dentate gyrus (DG) subregions, with high-magnification views of the corresponding areas shown on the right. Scale bars: low-magnification images, 100 μm; high-magnification images, 20 μm. (B–D) Quantitative analysis of the percentage of Nissl-positive cells in the hippocampal CA1, CA3, and DG subregions. (E) Representative images of NeuN immunohistochemical staining in hippocampal tissues from WT and KO mice. Rectangular boxes denote the CA1, CA3, and DG subregions, with high-magnification views of the corresponding areas shown on the right. Scale bars: low-magnification images, 100 μm; high-magnification images, 20 μm. (F–H) Quantitative analysis of the percentage of NeuN-positive immunoreactive area in the hippocampal CA1, CA3, and DG subregions. Data are expressed as mean ± SD (n=6 mice/group). Comparisons between two groups were analyzed using an unpaired two-tailed Student's t-test. *P < 0.05; **P < 0.01.

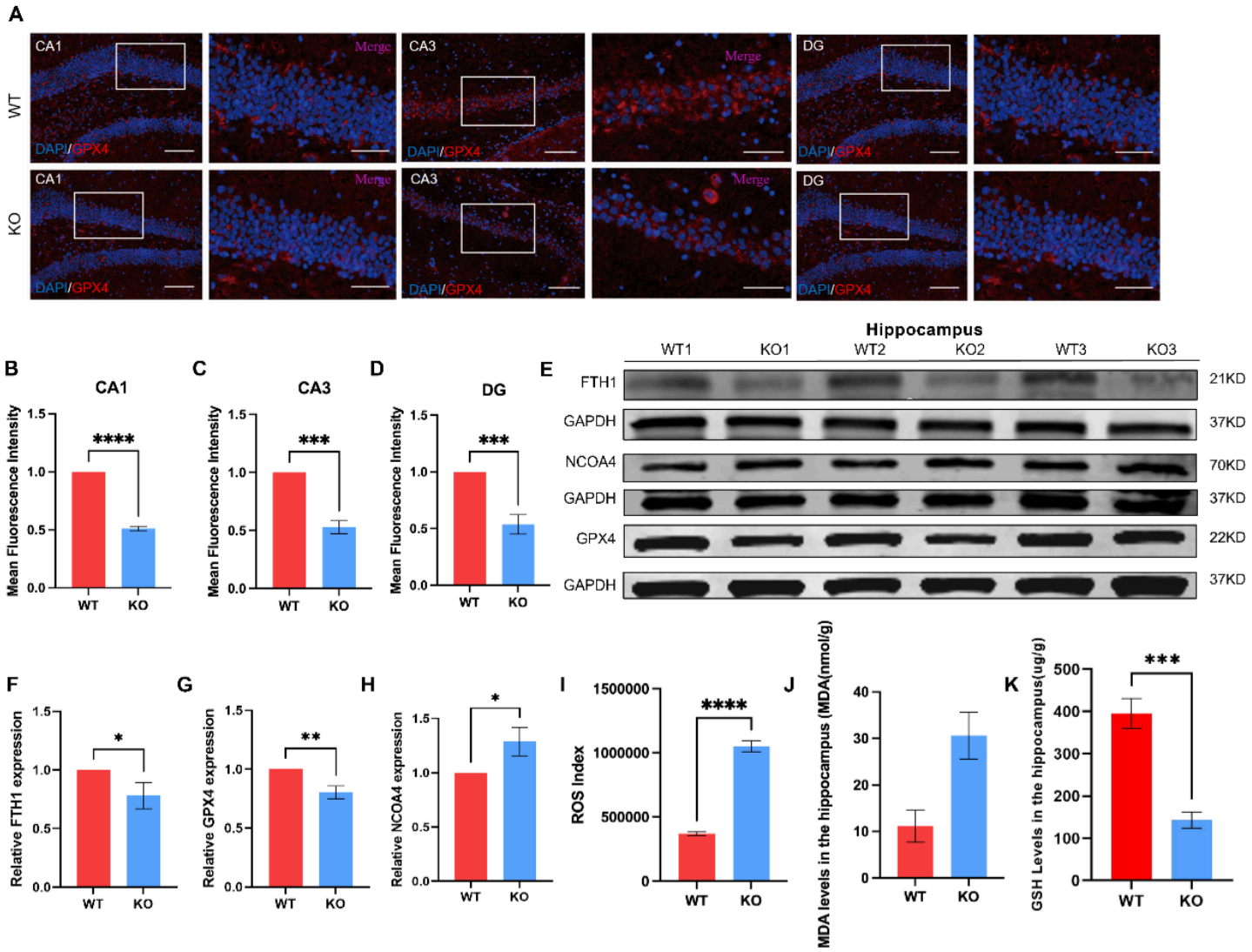


Figure 3

***Mex3c*deficiency downregulates GPX4 and FTH1 expression, upregulates NCOA4 expression, increases ROS and MDA levels, and decreases GSH content in the mouse hippocampus.**

(A) Representative immunofluorescence images of GPX4 in the hippocampal CA1, CA3, and dentate gyrus (DG) subregions of WT and KO mice. GPX4 is stained in red, and cell nuclei are counterstained with DAPI in blue. High-magnification views of the white boxed regions are shown on the right. Scale bars: low-magnification images, 500 μm; high-magnification images, 100 μm. (B–D) Quantitative analysis of the mean fluorescence intensity (MFI) of GPX4 in the hippocampal CA1, CA3, and DG subregions. (E) Representative Western blot images showing protein expression of FTH1, NCOA4, and GPX4 in hippocampal tissues of WT and KO mice, with GAPDH as the loading control. (F–H) Quantitative analysis of relative protein expression levels of FTH1, GPX4, and NCOA4. (I–K) Quantitative analysis of ROS levels, MDA content, and GSH content in hippocampal tissues of WT and KO mice. Data are expressed as mean ± SD (n=6 mice/group). Comparisons between two groups were analyzed using an unpaired two-tailed Student's t-test. *P< 0.05; **P < 0.01; ***P < 0.001; ****P < 0.0001.

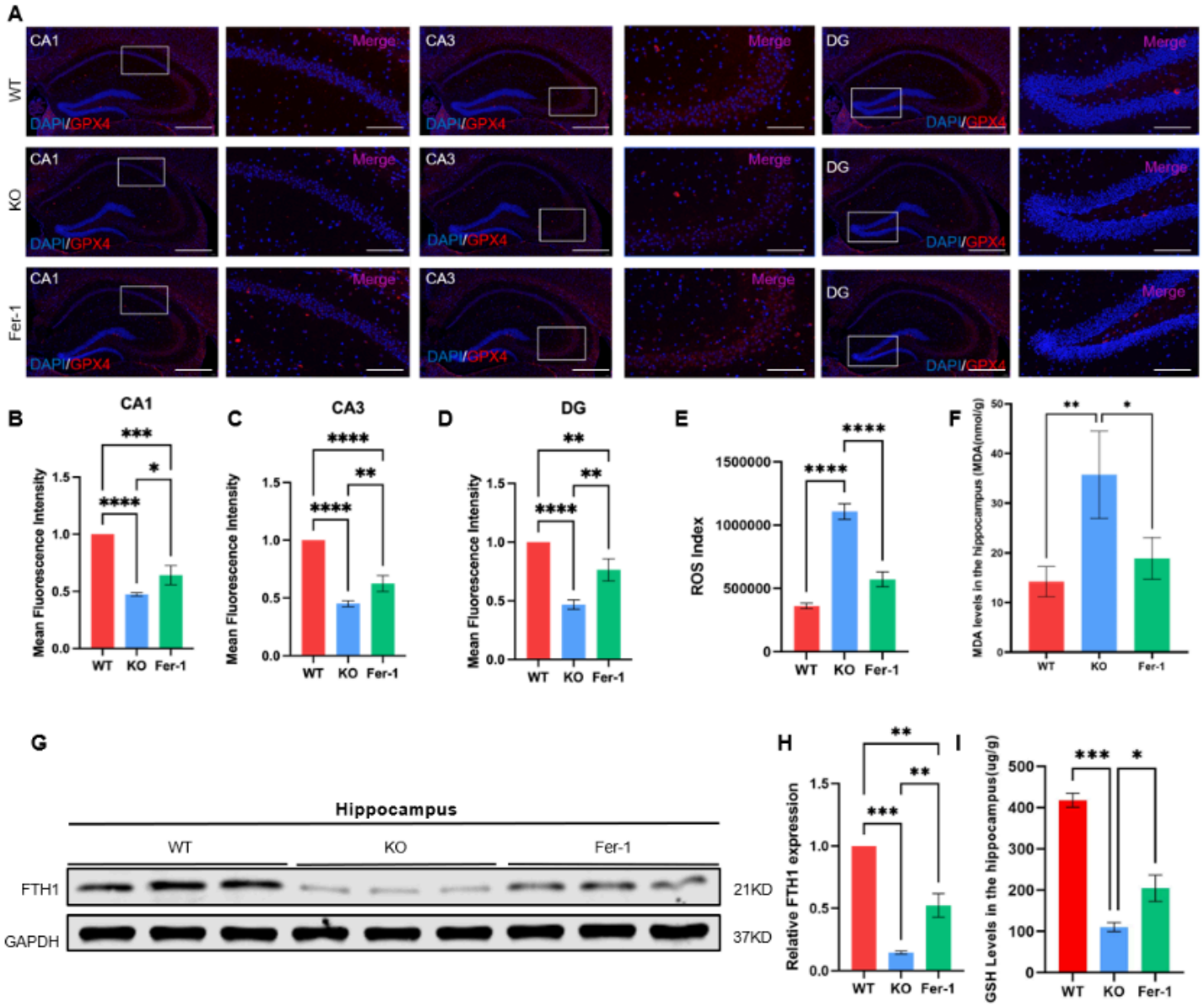


Figure 4

Fer-1 treatment partially reverses *Mex3c*deficiency-induced GPX4 and FTH1 downregulation, ROS and MDA elevation, and GSH depletion in the hippocampus.

(A) Representative immunofluorescence images of GPX4 in the hippocampal CA1, CA3, and dentate gyrus (DG) subregions of WT, KO, and KO + Fer-1 mice. GPX4 is stained in red, and cell nuclei are counterstained with DAPI in blue. High-magnification views of the white boxed regions are shown on the right. Scale bars: low-magnification images, 10 μm; high-magnification images, 20 μm. (B–D) Quantitative analysis of the mean fluorescence intensity (MFI) of GPX4 in the hippocampal CA1, CA3, and DG subregions. (E) Quantitative analysis of ROS levels in hippocampal tissues across groups. (F) Quantitative analysis of MDA content in hippocampal tissues across groups. (G) Representative Western blot images showing FTH1 protein expression in hippocampal tissues across groups, with GAPDH as the loading control. (H) Quantitative analysis of relative FTH1 protein expression levels. (I) Quantitative

analysis of GSH content in hippocampal tissues across groups. Data are expressed as mean ± SD (n=3 independent biological replicates/group). Comparisons among three groups were analyzed using one-way ANOVA followed by Tukey's post hoc multiple comparisons test. *P < 0.05; **P< 0.01; ***P < 0.001; ****P < 0.0001.

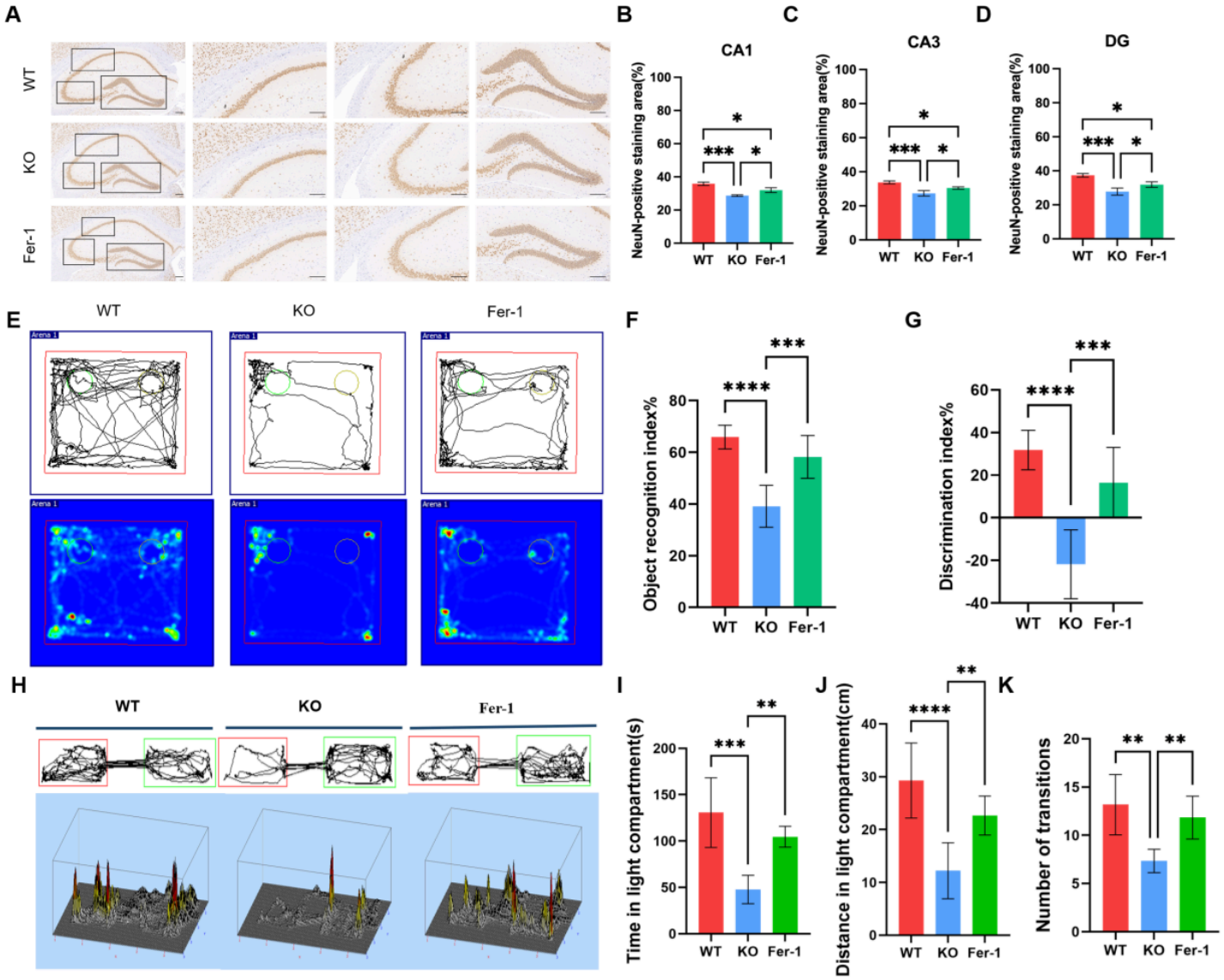


Figure 5

Fer-1 treatment partially restores hippocampal NeuN immunoreactivity and rescues recognition memory and anxiety-like behaviors in *Mex3c*-deficient mice.

(A) Representative images of NeuN immunohistochemical staining in hippocampal tissues from WT, KO, and KO + Fer-1 mice. Rectangular boxes denote the CA1, CA3, and dentate gyrus (DG) subregions, with high-magnification views of the corresponding areas shown on the right. Scale bars: low-magnification images, 100 μm; high-magnification images, 20 μm. (B–D) Quantitative analysis of the percentage of NeuN-positive immunoreactive area in the hippocampal CA1, CA3, and DG subregions. (E)

Representative locomotor trajectories and activity heatmaps of mice across groups in the novel object recognition (NOR) test. (F) Recognition index in the NOR test. (G) Discrimination index in the NOR test. (H) Representative locomotor trajectories and 3D activity heatmaps of mice across groups in the light-dark box (LDB) test. (I) Time spent in the light compartment. (J) Distance traveled within the light compartment. (K) Number of transitions between light and dark compartments. Data are expressed as mean ± SD (n=6 mice/group). Comparisons among three groups were analyzed using one-way ANOVA followed by Tukey's post hoc multiple comparisons test. *P < 0.05; **P < 0.01; ***P< 0.001; ****P < 0.0001.